Sensors & Transducers, Vol. 165, Issue 2, February 2014, pp. 61-67

www.sensorsportal.com

Sensors & Transducers

http://www.sensorsportal.com

An Automatic Wheel Contour Extraction Method

[1] Hui Zeng, [2] Han Wu, [3] Xiuqing Wang

[1] School of Automation and Electrical Engineering University of Science and Technology Beijing, Beijing 100083, China

[2] China National Computer Products Quality Supervising Test Center, Beijing 100083, China

[3] Vocational & Technical Institute, Hebei Normal University, Shijiazhuang 050031, China

[1] E-mail: hzeng@163.com

Received: 18 October 2013 /Accepted: 28 January 2014 /Published: 28 February 2014

Abstract: Wheel contour extraction from image is an important unit of any vision-based traffic accident analysis system, and automatically doing it is still a difficult task due to various distracting factors such as low contrast between the wheel and the ground, different wheel types and various weather conditions etc. In this work, a new automatic wheel extraction method is proposed, in which rather than directly extracting wheel contours from images, the wheel rim and the contacting image point of wheel to the ground are at first extracted, then the wheel contour is in turn located via the invariance of cross ratio. Extensive experiments under various weather conditions show that our proposed method is capable of detecting wheel contours fully automatically and robustly. *Copyright © 2014 IFSA Publishing, S. L.*

Keywords: Wheel contour, Wheel rim, Contacting image point, Harmonic conjugate, Cross ratio.

1. Introduction

Applying image processing and computer vision technology in the traffic accident analysis has attracted much attention in recent years [1-8]. Compared with the traditional investigation approaches, the vision based one has many advantages such as:

• It can save manpower and raise efficiency. Merely several images are needed to get related information of traffic accident scene.

• It can save time and help to dredge the roads as well as recover the traffic rapidly.

• The images of traffic accident scene can retain the evidence at the first hand so as to later get the missing information.

In the vision-based traffic accident analysis system, a variety of image features should be extracted, such as wheel contour, brake trace, the bloodstain etc. Their extraction accuracy will affect the measurement precision directly.

In this work, we are focused on the automatic extraction of wheel contours, an important unit of traffic accident analysis system. In fact, automatically and reliably extracting wheel contours from images is not an easy task due to various distracting factors, such as the wheel's thickness, texture, deformation, dust, and adverse weather conditions, as shown in Fig. 1. From these images, we can see that automatically extracting wheel contour is a difficult task. Since the wheel rim and tire have distinct differences in color and material, and it is relatively easy to extract the contour of wheel rim. Hence in this work, rather than directly extracting contour of wheels, we at first extract the contour of wheel rim and the contacting image point of wheel to the ground, by which, the contour of wheel is finally extracted via cross-ratio variance, and extensive experiments under various conditions

validate the robustness and good applicability of our "indirect" approach.

Fig. 1. Some wheel images.

2. System Calibration

Here by "system calibration", we mean to determine the vanishing line of the ground plane, denoted as l_∞, the vanishing point of lines perpendicular to the ground, denoted as v_z and the homography of the ground plane to the image, denoted as H_g. This is done by lying a specially designed "回"- type template on the ground, as shown in Fig. 2, then use line correspondences from the template to image to estimate the ground-to-image homography, and by which to compute the vanishing line and vanishing point. More specifically, we assume in this work only the focal length is subject to change and all other camera intrinsic parameters are pre-calibrated.

Fig. 2. Example of a test image.

Hence the ground-to-image homography can be expressed as:

$$H_g = \begin{pmatrix} f & 0 & 0 \\ 0 & f & 0 \\ 0 & 0 & 1 \end{pmatrix} (r_1 \quad r_2 \quad T) \tag{1}$$

and determined by the line correspondences, where $R=(r_1\ r_2\ r_3)$ and T is the rigid transformation from the world system with the ground plane at the (x,y) plane to the camera system [9, 10]. As shown in Fig. 3, the two vanishing points v_x, v_y of the ground plane are the intersecting points of the image lines of the parallel sides of the template, and

$$l_\infty = v_x \times v_y \tag{2}$$

$$v_z = Kr_3 = K(r_1 \times r_2) \tag{3}$$

The above is only a sketch, the interested reader is referred to Ref. [11] for more details.

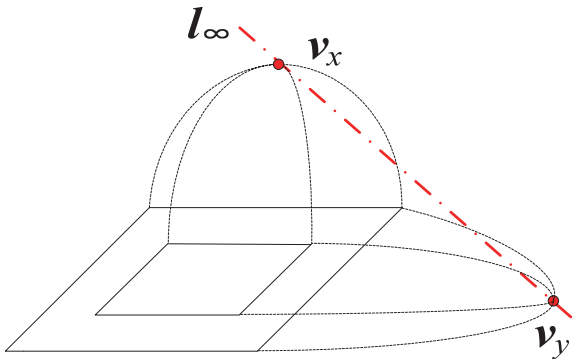

Fig. 3. He image of our "回"-type template and vanishing line, vanishing points.

3. Wheel Contour Extraction

For notational convenience, some key image features of wheel used in this work are shown in Fig. 4. A flowchart of our automatic wheel contour extraction method is shown in Fig. 5, and each one of the major steps will be elaborated as below.

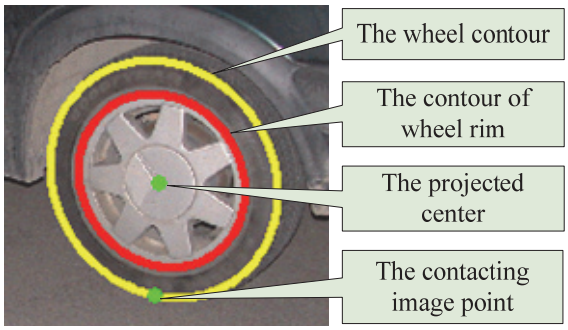

Fig. 4. The key image features of wheel.

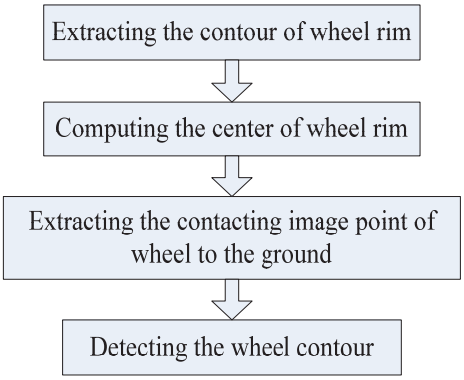

Fig. 5. Flowchart of our automatic extraction method.

3.1. Preprocessing

Hereinafter, a wheel image is meant in fact a small image region, not the whole image, interactively selected by the user, as shown in Fig. 6. At first, the original color image is converted to the gray-level image. Then we use image filtering techniques to reduce noise, and the result is shown in Fig. 6 (a). After that, we fill the black holes in the image to reduce the texture influence of the wheel rim. The result is shown in Fig. 6 (b). Then we reconstruct the image in order to reduce the influence of the tire texture and the background. As shown in Fig. 6 (c), the tire texture and the background in the reconstructed image become blurry. This processing step is to enhance the contour of the wheel rim and make it easy for the subsequent segmentation. All the techniques involved in this step are conventional ones, and details are omitted.

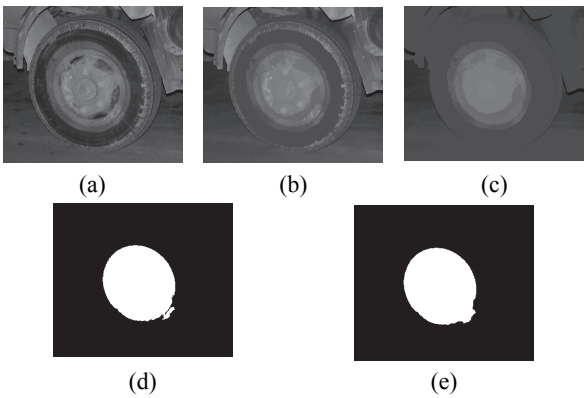

Fig. 6. The processed wheel images. (a) - filtered image, (b) - results after filling black holes, (c) - reconstructed image, (d) - binarized image, (e) - final result by a morphological filter.

3.2. Extraction of the Contour of Wheel Rim

The method in Ref. [12] is used to segment the wheel rim from the wheel image. The key is to select a suitable threshold. The following is our threshold selection process:

At first, the histogram of the wheel image is computed as *h*, where *h(i)* denotes the number of the pixels with gray value *i*. Define $t_0 = \frac{1}{256}\sum_{i=0}^{255} h(i)$, then some prominent points *(i, h(i))* on the histogram are selected if $|h(i)-h(i-1)| > t_0$. As shown in Fig. 7 and Fig. 8, the prominent points are labeled by red markers. The gray values of these prominent points are memorized in an array e.

After selecting the prominent points, the K-means clustering is used to cluster the gray values in the array *e* into three clusters, whose centers are labeled by green star-markers, as shown in Fig. 7 and Fig. 8 (a).

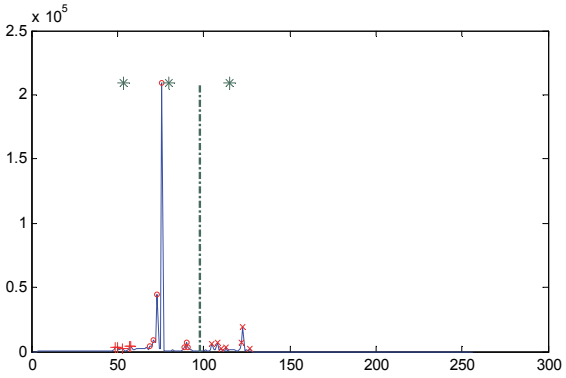

Fig. 7. Histogram based clustering when $M > \theta$.

Set their corresponding gray values are c_1, c_2 and c_3 ($c_1 < c_2 < c_3$), then a discriminant function is defined as:

$$M = \frac{c_3 - c_2}{c_2 - c_1} \tag{4}$$

If $M > \theta$ where θ is a preset threshold (in our work, it is always set to 0.3 regardless of images, and it is determined experimentally), then set the threshold $T = (c_2 + c_3)/2$. It is shown as green dot-lines in Fig. 7. If $M \le \theta$, the gray values are then clustered into two clusters, and $T = (c_1 + c_2)/2$, as shown in Fig. 8 (b).

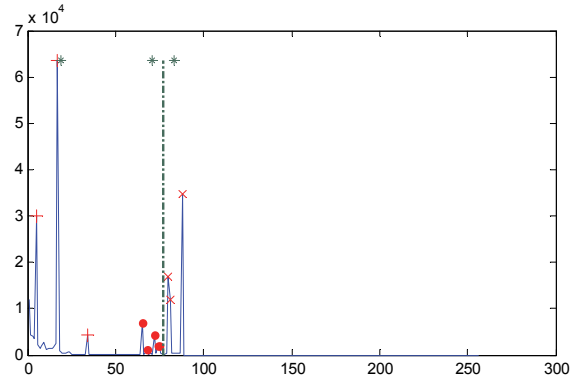

(a) results of three clusters when $M \le \theta$.

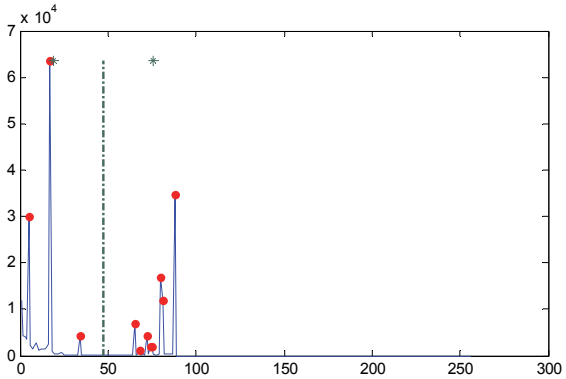

(b) results of two clusters when $M \le \theta$.

Fig. 8. Histogram based clustering when $M \le \theta$.

Finally the wheel image is binarized using the threshold T. The resulting binary image is shown in Fig. 6 (d). After some further morphological filtering and filling black holes, the result is shown as in Fig. 6(e).

After above segmentation, the segmented image is rather clean, and the contour of the wheel rim is extracted and fitted into an ellipse by conventional means [13]. In our work, the canny detector is used for edge detection, and the random sample consensus (RANSAC) technique is used for ellipse fitting [14]. The result is shown as the redpoints in Fig. 9.

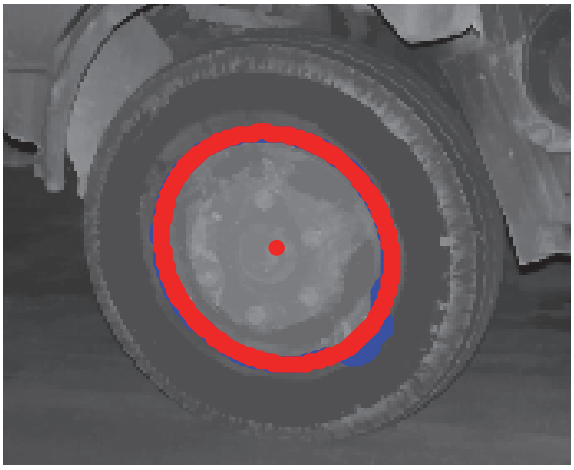

Fig. 9. Ellipse fitting.

3.3. Estimating the Projected Center of Wheel Rim

According to the theory of projective geometry, a circle projects to an ellipse in the image, but the projection of the circle's center is not always the center of the ellipse. In fact, the projected center of wheel rim can be located as follows.

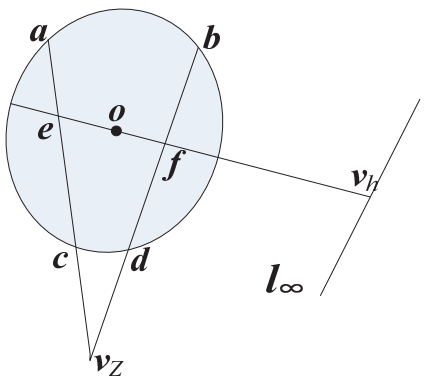

Fig. 10. Computing the projection of the circle's center of on the image.

As shown in Fig. 10, selecting arbitrarily two points a and b on the ellipse. The line passing through point a and vertical vanishing point v_z intersects the ellipse at point c. Similarly the line passing through point b and v_z intersects the ellipse at point d. Then we can obtain two chords ac and bd. Since both line ac and bd pass through the vertical vanishing point v_z, their corresponding 3D line segments (denoted as AB, CD) must both be perpendicular to the ground. Suppose the midpoint of AC is point E, its projection is e, then points (a, c) and (e, v_z) must be pairs of harmonic conjugates (Hartley and Zisserman, 2003), then point e can be located by:

$$cross(a, c, e, v_z) = -1 \tag{5}$$

Similarly the projection f of the midpoint of segment BD can be located. Suppose line ef intersects the vanishing line l_∞ at v_h, once again, (e, f) and (o, v_h) constitute pairs of harmonic conjugates. Hence the projected center of wheel rim can be located by:

$$cross(e, f, o, v_h) = -1 \tag{6}$$

In practice, we find that the center of the ellipse can be reliably considered as the projected center o of wheel rim. Sometimes, the computed center as outlined in the above is error-prone due to possible errors in the estimated vanishing line and vanishing points. As shown in Fig. 13, the red-dot marker is the center of the ellipse and the yellow-star marker is the projection of wheel rim center estimated by the above procedure. We can see that the two points are very close to each other.

3.4. Extracting the Contacting Image Point of Wheel to the Ground

Here by "contacting image point" is meant the projected image point of the contacting point of wheel to the ground. Detecting the contacting image point at first, then using it to extract the contour of wheel, is the major novelty of our work and the key contributor of our success of wheel contour extraction. The underlying principle is rather simple. The contacting image point, which is constrained on a line, is much easier to detect than to directly extract the contour of wheel from image. It is done as follows.

The contacting image point must lie on the line l_c defined by vertical vanishing point v_z and the projected center o of wheel rim since the contour of wheel rim and wheel contour are two concentric circles, and the contacting point of wheel to the ground is the intersecting point of the vertical line from the center of wheel rim to the ground. From the point o and along the line l_c directing to the ground,

we search a point with the greatest gradient variance and this point is considered as the contacting image point of wheel to the ground.

In order to further enhance the detection robustness, some gray constraints on a small neighborhood of the contacting image point m_t are also used. For example, before reaching the contacting image point from the point o, a small interval of black pixels should appear. After the contacting image point, there should exist a small interval of pixels having similar gray values, but noticeably different from that of the contacting image point. A detection result is shown in Fig. 11.

Fig. 11. The contacting image point of wheel to the ground.

3.5. Detecting the Wheel Contour

So far we have obtained the contour of wheel rim, the center of wheel rim and the contacting image point of wheel to the ground, our final step is to detect the wheel contour using the above obtained information. As shown in Fig. 12, the line om_t intersects the contour of wheel rim at the point j and k. Suppose mn is the projection of a diameter of the 3D real wheel rim and it intersects the wheel contour at point q. The cross ratio of points o, q, m, n equals to the cross ratio of points o, m_t, j, k, so we can compute the coordinates of point q by:

$$cross(o,q,m,n) = cross(o,m_t,j,k) \tag{7}$$

In the same way, we can compute other points on the wheel contour. A result is shown in Fig. 13.

4. Experimental Results

A test set of 201 images is used in our experiment. All the images are taken by a Nikon Coolpix 5700 digital camera with the resolution of 2560×1920 at different time and under various weather conditions. 77 images are taken in the sunny condition, 23 images in the cloudy condition, 39 images in the rainy condition and 62 images in the evening. We first use canny edge detector to detect the edge points of the reference template. Then we use a least-squares technique to fit the detected edge points into lines, and the ground plane to image homography is estimated by line correspondences from the template to image, then vanishing point and vanishing line are computed as outlined in Section 2. Finally we use our method to detect the wheel contour. Due to the space limit, here we only report the experimental results of six test images, others are listed in Table 1.

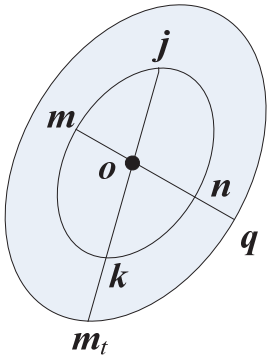

Fig. 12. Detecting the wheel contour.

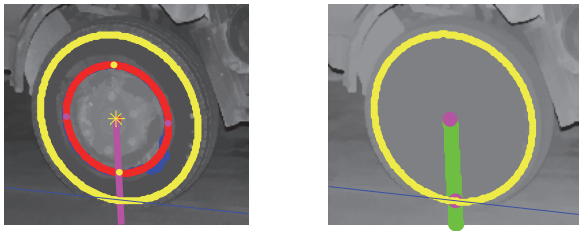

Fig. 13. Extracted contours.

Table 1. The experimental results of the test image set.

	Test Image Number	Correct Number	Error Number
Sunny	77	63	14
Cloudy	23	20	3
Rainy	39	37	2
Evening	62	53	9
Total Number	201	173	28

In Table 1, whether a detection result is successful is subjectively judged by a human operator. As shown in Fig. 14 (a) is a cloudy image, Fig. 14 (b) and Fig. 14 (c) are images in the evening, Fig. 14 (d) and Fig. 14 (e) are rainy images and Fig. 14 (f) is a sunny image. The two green dots are the center of wheel rim and the contacting image point of wheel to the ground respectively. The red ellipse is the contour of the wheel rim and the yellow

ellipse is the wheel contour. The magenta line is the line passing through the center of wheel rim and the vertical vanishing point. From these figures and the results in Table 1, we can see that our proposed method performs fairly well.

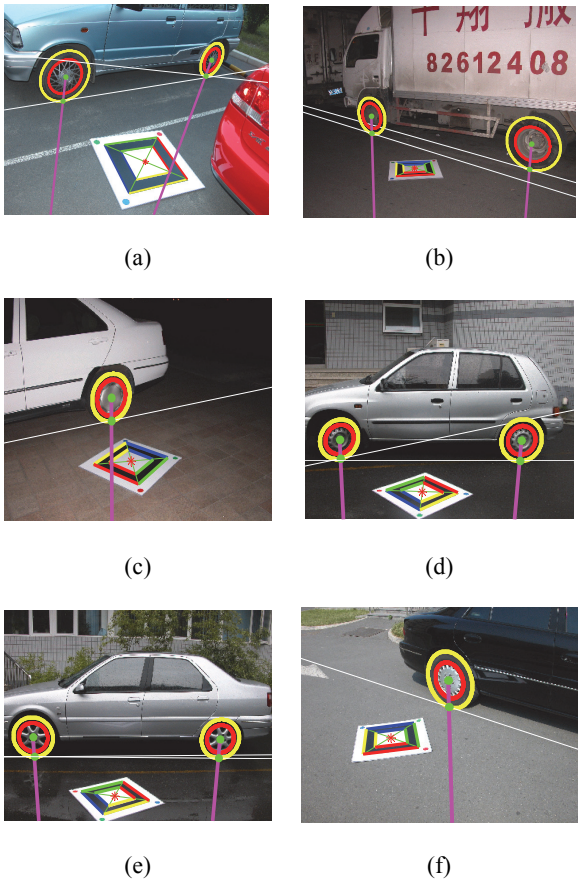

(a) (b) (c) (d) (e) (f)

Fig. 14. Extracted contours under various weather conditions.

Of course, some errors inevitably exist in the estimated vanishing point, vanishing line and contacting image point. However our experiments show that such errors are not too damaging as long as they are not too excessive. As shown in Fig. 13, although the estimated contacting point is not accurate enough, it is still on the wheel contour and the cross ratio relationship still preserves, and the wheel contour can still be detected using this inaccurate contacting point.

5. Conclusions

The wheel contour extraction is an important unit in the traffic accident analysis system. In this paper, an indirect approach, which at first detects the contacting image point of the wheel to the ground, then extracts wheel contours via cross ratio invariance, is proposed and validated by extensive experiments under various weather conditions. Our proposed approach is fully automatic and robust.

Before ending this section, we would point out that although the detection of vanishing points and vanishing lines is notoriously sensitive to noise, this problem is not too serious in our case since we used a carefully designed "回"- type template to compute these infinity entities in our system calibration step.

Acknowledgements

This paper is supported by the National Natural Science Foundation of China under the Grant No. 61005009, 61175059 and 61170116, and the Fundamental Research Funds for the Central Universities under the Grant No. FRF-TP-12-100A.

References

[1]. Kantawong S., Phanprasit T., Intelligent traffic cone based on vehicle accident detection and identification using image compression analysis and RFID system, in *Proceedings of the International Conference on Electrical Engineering / Electronics Computer Telecommunications and Information Technology*, 2010, pp. 1065-1069.

[2]. Jing-Lei Zhang, Bin Gao, Xiu-Ping Gu, Traffic images enhancement based on vanishing point detection and atmospheric scattering model, in *Proceedings of the International Congress on Image and Signal Processing,* 2, 2010, pp. 766-770.

[3]. Heidari V., Ahmadzadeh M. R., A method for vehicle classification and resolving vehicle occlusion in traffic images, in *Proceedings of the 1st Iranian Conference on Pattern Recognition and Image Analysis*, 2013, pp. 1-6.

[4]. Jun-Tao Xue, Cui-Rong Wang, Shao-Fang Xing, Dual background modeling of traffic image based on LBP and Gaussian, in *Proceedings of the International Conference on Machine Learning and Cybernetics*, 4, 2012, pp. 1362-1366.

[5]. Zhang K., Sheng Y., Li J., Automatic detection of road traffic signs from natural scene images based on pixel vector and central projected shape feature, *IET Intelligent Transport Systems*, 6, 3, 2012, pp. 282-291.

[6]. Jianming H., Qiang M., Qi W., Jiajie Z., Yi Z., Traffic congestion identification based on image processing, *IET Intelligent Transport Systems*, 6, 2, 2012, pp. 153-160.

[7]. Somasundaram G., Sivalingam R., Morellas V., Papanikolopoulos N., Classification and Counting of Composite Objects in Traffic Scenes Using Global and Local Image Analysis, *IEEE Transactions on Intelligent Transportation Systems*, 14, 1, 2013, pp. 69-81.

[8]. Ye Li, Bo Li, Bin Tian, Qingming Yao, Vehicle Detection Based on the and-or Graph for Congested Traffic Conditions, *IEEE Transactions on Intelligent Transportation Systems*, 14, 2, 2013, pp. 984-993.

[9]. Zhengyou Zhang, A flexible new technique for camera calibration, *IEEE transactions on Pattern Analysis and Machine Intelligence*, 22, 11, 2000, pp. 1330-1334.

[10]. Richard Hartley, Andrew Zisserman, Multiple View Geometry in Computer Vision (Second Edition), *Cambridge University Press*, 2003.

[11]. Fengrong Huang, Zhanyi Hu, Yihong Wu, A New Method on Single View Metrology, *Acta Automatica Sinica,* 30, 4, 2004, pp. 487-495.
[12]. Gonzalez R. C., Woods R. E., Digital Image Processing (Second Edition), *Prentice Hall*, 2002.
[13]. Fitzgibbon A. W., Pilu M., Fisher R. B., T. More, Direct least-squares fitting of ellipses, *IEEE Transactions on Pattern Analysis and Machine Intelligence,* 21, 5, 1999, pp. 476-480.
[14]. Fischler M. A., Bolles R. C., T. More, Random Sample Consensus: A Paradigm for Model Fitting with Applications to Image Analysis and Automated Cartography, *IEEE Transactions on Pattern Analysis and Machine Intelligence, Comm. of the ACM*, 24, 6, 1981, pp. 381-395.